Temperature-Dependent Macroscopic Mechanical Behaviors and Their Microscopic Explanations in a Medium Mn Steel

JIAWEI MA, HAITING LIU, QI LU, YONG ZHONG, LI WANG, and YAO SHEN

Plastic instability (*e.g.*, Lüders band and PLC band) is a phenomenon frequently observed in cold-rolled medium Mn steels. In this study, through a number of quasi-static uniaxial tensile tests with digital image correlation (DIC) measurement of the strain rate field, we found the medium Mn steel (Fe-0.14C-7.14Mn-0.23Si wt. pct with approximately 33 vol pct of retained austenite and 67 vol pct of ferrite) exhibited distinct competition/coordination between the Lüders band and the PLC band at different deformation temperatures: (1) at 25 °C and 55 °C, a Lüders band was followed by several PLC bands; (2) at 100 °C, fracture occurred right after the Lüders band formation, without the presence of a PLC band; (3) at 250 °C, only PLC bands were observed. We propose that these macroscopic behaviors can be explained by the temperature-dependent conditions for the formation/appearance and propagation of Lüders bands and PLC bands. The propagation of Lüders bands becomes difficult when the temperature increases as less hardening is provided by martensitic transformation. In contrast, the appearance and propagation of PLC bands become easier when the temperature increases and/or the plastic strain becomes large (16.5 and 18.9 pct in this material at the deformation temperatures of 25 °C and 55 °C, respectively), as the difference in the average velocities of solute atom diffusion and dislocation gliding is reduced. Either condition for Lüders bands or for PLC bands will be satisfied at different deformation temperatures or plastic strains, thus leading to the competition/coordination between them.

https://doi.org/10.1007/s11661-020-05958-z

I. INTRODUCTION

In recent years, medium Mn steels, as promising candidates for the third-generation advanced high strength steels with excellent combinations of high strength and large elongation (compared to common TRIP steels[1]), have been investigated extensively.[1–5] Their excellent mechanical properties mainly originate from the large volume fraction of metastable austenite, typically ranging from 20 to 40 pct, which will transform into martensite during deformation and provide extra work hardening ability to improve the elongation by delaying the necking stage. However, some plastic instability phenomena, such as Lüders bands and/or Portevin-Le Châtelier (PLC) bands, have been reported in cold-rolled medium Mn steels when deformed at different temperatures.[6–10] These phenomena, unfortunately, may give rise to stretcher-strain marks on steel surfaces and influence sheet forming performance.[11] In order to suppress or even eliminate these undesirable phenomena, it is imperative to investigate the different macroscopic mechanical behaviors involved at various deformation temperatures and the underlying microscopic explanations.

When cold-rolled medium Mn steels are deformed at various temperatures during quasi-static uniaxial tensile tests, the competition/coordination between the Lüders band and the PLC band has been frequently observed.[6–8] At certain temperatures, both types of bands may co-exist, while at some other temperatures, one type of bands will take the dominant role. For example, when Wang *et al.*[7] examined the tensile behaviors of a Fe-7Mn-0.14C-0.23Si (wt. pct) steel at room temperature (RT), 100 °C and 300 °C, respectively, they found a Lüders band at each of these temperatures, yet only PLC bands (corresponding to the remarkable stress serrations on the tensile curve) at RT after the propagation of the Lüders band. Also, when investigating the tensile behaviors of a

JIAWEI MA, HAITING LIU, and YAO SHEN are with the School of Materials Science and Engineering, Shanghai Jiao Tong University, Shanghai 200240, China. Contact e-mail: yaoshen@sjtu.edu.cn QI LU is with the China Science Lab, General Motors Global Research and Development, Shanghai 201206, China. Contact e-mail: qi.lu@gm.com YONG ZHONG and LI WANG are with the State Key Lab of Development and Application Technology of Automotive Steels, Baosteel Research Institute, Shanghai 201900, China.

Manuscript submitted 18 November 2019.
Article published online August 20, 2020

Fe-7Mn-0.3C-2Al (wt. pct) steel and a Fe-10Mn-0.1-C-2Al (wt. pct) steel at -50 °C, RT and 100 °C, respectively, Yang *et al.*[6] and Zhang *et al.*[8] reported similar findings.

To better understand these plastic instability phenomena, some microscopic explanations have been proposed. So far it has been generally accepted that Lüders bands are formed due to the lack of mobile dislocations, and the amount of mobile dislocations might be reduced after the intercritical annealing process in cold-rolled medium Mn steels.[4,12,13] To maintain the propagation of Lüders bands, sufficient strain hardening ability is needed, which can be provided by martensitic transformation during deformation.[8,14–16] However, martensitic transformation seems not to be a necessary condition for the appearance of PLC bands. Sun *et al.*[17] and Abu-Farha *et al.*[18] observed localized martensitic transformation within the PLC band fronts in a Fe-0.2C-10.3Mn-2.9Al (wt. pct) steel and a Fe-0.15C-10.0Mn-1.5Al-0.2Si (wt. pct) steel, respectively. By contrast, Wang *et al.*[19] reported that there was almost no martensitic transformation during the propagation of the PLC bands in a Fe-7Mn-0.14C-0.23Si (wt. pct) steel. Still, after examining a Fe-7Mn-0.3C-2Al (wt. pct) steel, Yang *et al.*[6] suggested that the PLC bands in this steel might originate from the interaction between C atoms/C-Mn pairs and mobile dislocations in austenite.

Nevertheless, the studies above focused either on Lüders bands or PLC bands. A unified microscopic explanation for the competition/coordination between them, was rarely reported. Therefore, in this study, we conducted quasi-static uniaxial tensile tests with DIC measurement of the strain rate field in a cold-rolled medium Mn steel (Fe-0.14C-7.14Mn-0.23Si wt. pct) at different deformation temperatures (25 °C, 55 °C, 100 °C and 250 °C, respectively) to investigate the macroscopic behaviors of the Lüders band and the PLC band. Then, we proposed a unified microscopic explanation for these distinct temperature-dependent macroscopic behaviors, including the competition/coordination between the bands.

II. EXPERIMENTAL PROCEDURE

The medium Mn steel (provided by Baosteel) employed in our experiments has a chemical composition of Fe-0.14C-7.14Mn-0.23Si (wt. pct). It was produced by intercritical annealing at a temperature around 620 °C for 3 minutes after cold rolling. Its microstructure was characterized by Electron Backscatter Diffraction (EBSD) and Transmission Electron Microscopy (TEM). EBSD maps were captured in a Zeiss™ Auriga SEM equipped with an Oxford™ EBSD detector at an accelerating voltage of 20 kV and a step size of 50 nm. TEM images were taken in a Joel™ 2100F transmission electron microscope at 200 kV, and the specimen was prepared by twin-jet electropolishing at a temperature of − 20 °C with a solution of 10 vol pct perchloric acid and 90 vol pct ethanol. Quasi-static uniaxial tensile tests were conducted at various deformation temperatures, ranging from 25 °C to 250 °C, in an Instron™ mechanical testing machine equipped with an environmental chamber at an applied cross-head speed of 0.6 mm/min (corresponding to a nominal strain rate of 2×10^{-4}/s). Dog-bone-shaped tensile specimens were cut along the rolling direction, with a gauge length of 50 mm (according to the AS™ E8 standards). These specimens were held for 20 minutes to reach the target temperature and maintain a homogeneous temperature distribution. The digital image correlation (DIC) method was utilized to characterize these plastic instability phenomena during the tensile tests. Two digital cameras (in a stereo DIC system) with 35 mm lenses were set to focus on all areas of interest (50 mm × 10 mm, denoted by the red dashed box in Figures 3 through 6), to capture the evolution of the randomly distributed black-white patterns on the surface of each specimen. Furthermore, all the patterns were produced with an airbrush. The frame rate and the exposure time of the camera were set at 0.8 frame/s and 25 ms, respectively. Post-processing was conducted with the Vic-3D software of Correlated Solutions™, Inc. The subset size and the grid point spacing were set at 15 × 15 pixel^2 and 5 pixel, respectively. The engineering strains on the tensile curves were measured by a 50mm virtual extensometer in this software. The effect of the deformation temperature on the accuracy of the DIC measurement was evaluated in the Appendix A. In addition, some tensile tests were interrupted to obtain the specimens for measuring the volume fraction of retained austenite by XRD after the propagation of the Lüders band or the PLC band. These XRD tests were conducted in a Bruker™ D8 ADVANCE X-Ray diffractometer with Co Kα radiation. The volume fraction of retained austenite was determined by Eq. [1][20] as follows, in which, I_γ is the average integrated intensity of (200)γ, (220)γ and (311)γ, and I_α is the average integrated intensity of (200)α and (211)α.

$$V_\gamma = \frac{1.4I_\gamma}{I_\alpha + 1.4I_\gamma} \quad [1]$$

III. RESULTS

As shown in Figure 1(a), the microstructure of the medium Mn steel employed in our experiments is composed of an ultrafine ferritic matrix and ultrafine retained austenite grains (approximately 33.0 vol pct measured by XRD). The EBSD analysis indicates that the grain size of ferrite and retained austenite is, respectively, 0.57 and 0.38 μm. In addition, as demonstrated in the TEM bright-field image (Figure 1(b)), the initial dislocation density is quite low in both phases after the intercritical annealing process.

Tensile curves obtained at different deformation temperatures are plotted in Figure 2, and the corresponding DIC-measured evolution of the equivalent strain rate distribution in the tensile specimens are illustrated in Figures 3 through 6. According to these

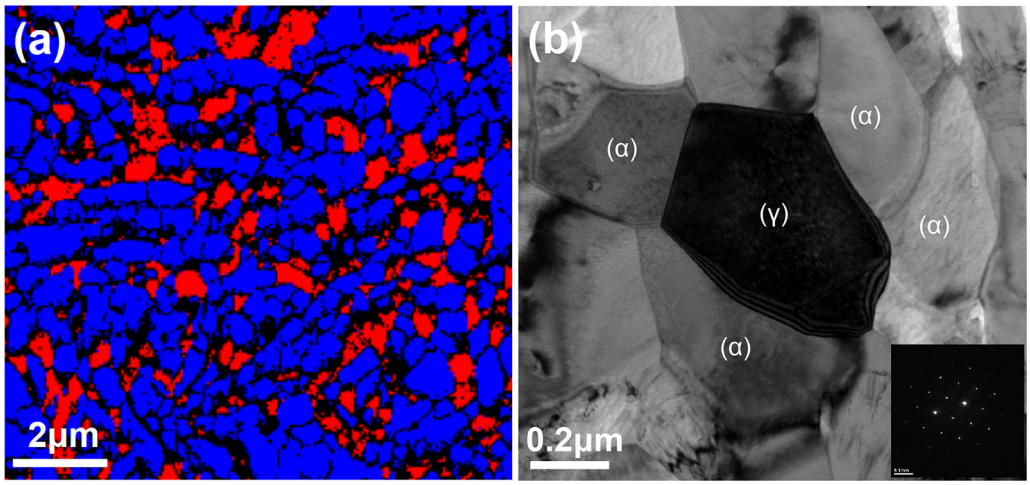

Fig. 1—(*a*) EBSD phase map (ferrite in blue and austenite in red), and (*b*) bright-field TEM image of the microstructure of our medium Mn steel.

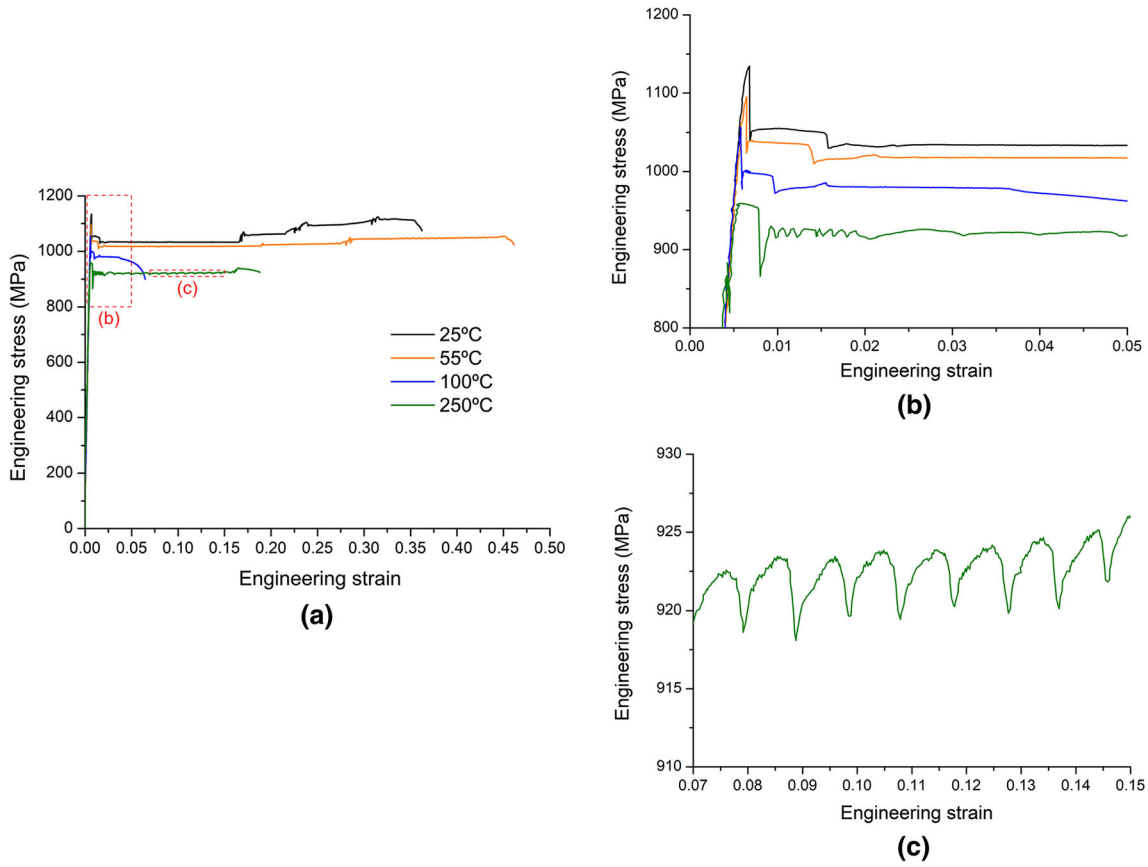

Fig. 2—(*a*) The temperature-dependent engineering stress-strain curves of the medium Mn steel with an applied cross-head speed of 0.6 mm/min (corresponding to a nominal strain rate of 2×10^{-4}/s), (*b*) and (*c*) are the magnifications of some parts in (a).

figures, plastic instability phenomena (*e.g.*, Lüders band and PLC band) existed at different temperatures and presented unique temperature-dependent features, especially the distinct competition/coordination between the Lüders band and the PLC band, which is quite different from the previous results.[6–8]

Specifically, at the deformation temperatures of 25 °C and 55 °C, a Lüders band was followed by several PLC bands. As shown in Figure 2, a long stress plateau appeared right after the sharp yield point drop, which indicated the nearly steady-state propagation of the Lüders band (Figures 3 and 4). The Lüders strain at

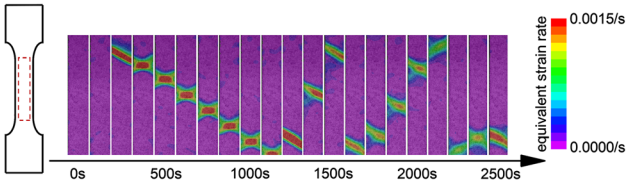

Fig. 3—The DIC-measured evolution of the equivalent strain rate distribution in the region denoted by the red dashed box with time when the specimen is deformed at 25 °C (Color figure online).

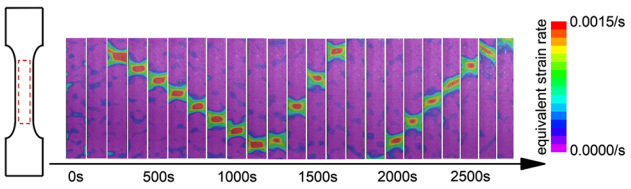

Fig. 4—The DIC-measured evolution of the equivalent strain rate distribution in the region denoted by the red dashed box with time when the specimen is deformed at 55 °C (Color figure online).

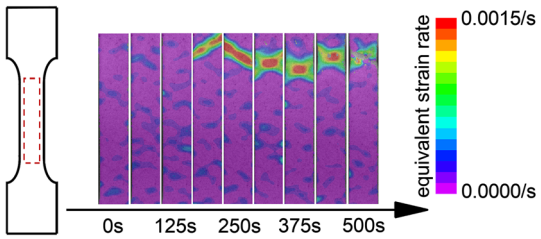

Fig. 5—The DIC-measured evolution of the equivalent strain rate distribution in the region denoted by the red dashed box with time when the specimen is deformed at 100 °C (Color figure online).

these two temperatures were 16.5 and 18.9 pct, respectively. Once the Lüders band passed through the whole gauge length, type A PLC bands emerged, which were displayed as step-like behaviors on the tensile curves (Figure 2). They all nucleated at one end of the gauge length and propagated continuously to the other in sequence, exhibiting the characteristics of the type A PLC band.[21,22]

At the deformation temperature of 100 °C, however, fracture occurred right after the Lüders band formation, without the presence of a PLC band. As shown in Figure 5, early necking initiated rapidly after the Lüders band formation. Accordingly, there existed a quite low elongation of 6.5 pct and no detectable Lüders strain, which was quite different from those at 25 °C and 55 °C.

Then at the deformation temperature of 250 °C, only PLC bands were observed (without the presence of a Lüders band) during the whole plastic deformation. The tensile curve exhibited several distinct stress serrations (with an amplitude of approximately 5 MPa), which initiated right after yielding and disappeared at approximately 16.0 pct engineering strain. As illustrated in Figure 6, a band with inclined front nucleated at one end of the specimen, whose orientation switched symmetrically during its propagation. Each switch

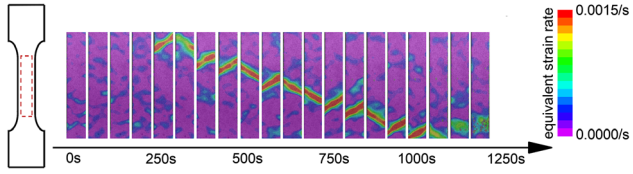

Fig. 6—The DIC-measured evolution of the equivalent strain rate distribution in the region denoted by the red dashed box with time when the specimen is deformed at 250 °C (Color figure online).

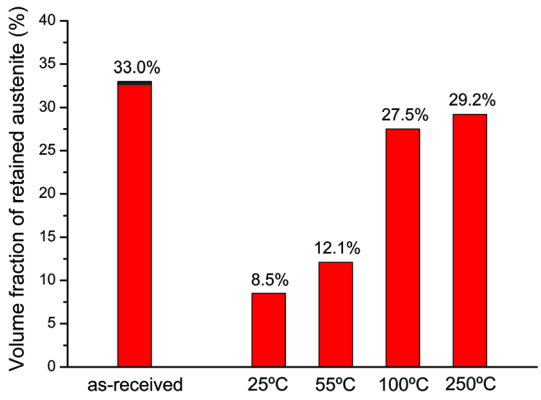

Fig. 7—The volume fraction of retained austenite in the as-received specimen, in the specimens right after the propagation of the Lüders band (25 °C, 55 °C, 100 °C), and in the specimen after the propagation of the PLC band (250 °C).

corresponded to a stress serration on the tensile curve. After the band arrived at the other end of the gauge length, no more bands appeared, but necking developed rapidly. Given these features, this propagative band was believed to be the PLC band.

Moreover, to explore the effect of the martensitic transformation on these bands, we compared the volume fraction of retained austenite before and after the propagation of the Lüders band (25 °C, 55 °C and 100 °C) or the PLC band (250 °C) in these specimens. As summarized in Figure 7, the volume fraction of retained austenite after the propagation of these propagative bands was obviously temperature dependent. While large amounts of retained austenite transformed into martensite when deformed at 25 °C and 55 °C, there was less martensitic transformation at 100 °C and 250 °C.

IV. DISCUSSION

To interpret these distinct temperature-dependent macroscopic features in our medium Mn steel, here we propose a unified microscopic explanation.

As is well accepted, the Lüders band formation originates from the insufficient mobile dislocations in the initial microstructure for carrying out plastic deformation.[23] When the upper yielding stress is reached, large amounts of mobile dislocations will be generated, thus leading to local strain localization and formation of a Lüders band. This mechanism can well explain the

Lüders band formation in our medium Mn steel, since the initial dislocation density is quite low in both phases after the intercritical annealing process, as demonstrated in the TEM bright-field image (Figure 1(b)).

Moreover, enough local strain hardening ability is generally believed to be the condition for suppressing the further growth of the local plastic instability and maintaining the Lüders band propagation. Although strain hardening ability could be provided by the ferritic matrix, it is not enough on many occasions, especially in materials with ultrafine grains. Instead, we propose that martensitic transformation can also provide extra strain hardening. As martensitic transformation is generally believed to introduce: (1) hard martensite with high dislocation density, (2) high density of geometrically necessary dislocations (GNDs) in adjacent ferrite grains to accommodate the volume expansion brought by martensitic transformation,[24,25] it could be inferred from the dislocation theory that martensitic transformation could provide extra strain hardening by two ways[14]: firstly, these high-density GNDs which are difficult to be eliminated by mutual annihilation, would work as obstacles to hinder the glide of mobile dislocations in ferrite grains, thus providing extra strain hardening ability. Secondly, the plastic deformation of these hard martensite with high dislocation density could also contribute to that by dislocation strengthening.

Therefore, the stability of retained austenite is a critical factor for interpreting these temperature-dependent Lüders band behaviors in our medium Mn steel. At 25 °C and 55 °C, the stability of retained austenite at 55 °C was a bit higher than that at 25 °C, and thus enough GND hardening was accumulated till a larger strain. This then resulted in a slight increase of Lüders strain along with the increase of the deformation temperature (from 16.5 pct at 55 °C to 18.9 pct at 25 °C, as shown in Figure 2). At 100 °C, given the much higher stability of retained austenite (Figure 7), only little martensitic transformation occurred. Thus, the hardening from martensitic transformation was undoubtedly not enough to support the propagation of the Lüders band. Hence, early fracture appeared. However, at 250 °C, even though very little martensitic transformations occurred, owing to the high diffusion velocity of solute atoms at this temperature, the Lüders band was replaced by the PLC band, which would be discussed below.

The temperature-dependent PLC band behaviors could be interpreted in the framework of classic dynamic strain aging (DSA) theory.[26–29] It depicts a microscopic scenario in which gliding dislocations repetitively interact with solute atoms (repeated pinning and depinning). The condition for this mechanism to work is to have comparable average velocities of solute atom diffusion and dislocation gliding. The velocity of solute atom diffusion is strongly controlled by temperature. The velocity of dislocation gliding, according to the Orowan equation ($\dot{\varepsilon} = \rho_m b \upsilon$), however, is affected by the mobile dislocation density when the strain rate is set.

Then, the distinct competition/coordination between the Lüders band and the PLC band at various deformation temperatures could be well explained by examining which condition is satisfied at a specific deformation temperature. Specifically, at 25 °C and 55 °C, due to the low diffusion velocity of solute atom (lower than that of dislocation gliding), the PLC bands could not initiate at the early stage of plastic deformation. However, a Lüders band appeared because of the low initial mobile dislocation density and the extra strain hardening ability provided by martensitic transformation. During the Lüders band propagation, the resulting large amounts of martensitic transformation and the significant increase of plastic strain introduced a much higher mobile dislocation density. Based on the Orowan equation, the average velocity of mobile dislocations would decrease since the applied strain rate was set. Then, the average velocities of dislocation gliding and solute atom diffusion became comparable, leading to the development of the PLC bands after the propagation of a Lüders band. At 100 °C, with little martensitic transformation, neither the fast diffusion velocity of solute atoms nor the above significantly decreased gliding velocity of mobile dislocations, was satisfied. Consequently, the significant difference in velocity between them hindered the appearance of PLC bands at the early stage of plastic deformation. In addition, though the Lüders band could initiate, it could not propagate, due to the lack of hardening provided by martensitic transformation. Therefore, the material fractured early. At 250 °C, the velocity of solute atom diffusion was significantly increased, thus being capable of interacting with gliding dislocations repetitively. In this case, only PLC bands were observed (without the presence of a Lüders band) during the whole plastic deformation.

Additionally, the experimental results also indicate that martensitic transformation might not be the necessary condition for PLC bands, which echoes the findings of some previous studies.[19,30] For the medium Mn steel employed in this study, although martensitic transformation would contribute to the development of PLC bands at the deformation temperatures of 25 °C and 55 °C (by introducing high mobile dislocation density to lower the average velocity of these mobile dislocations), PLC bands were still observed at 250 °C when little austenite transformed into martensite. This indicates that martensitic transformation is not necessary for PLC bands at this deformation temperature.

V. CONCLUSIONS AND SUMMARY REMARKS

In summary, we have found that the macroscopic mechanical behaviors in a cold-rolled medium Mn steel are uniquely temperature-dependent, and attempted a consistent microscopic explanation for such behaviors. Our explanation highlights two controlling factors: (1) martensitic transformation provides straining hardening for the Lüders band, (2) the difference in the average velocities of solute atom diffusion and dislocation gliding determines the appearance/propagation of the PLC band. At different deformation temperatures or plastic strains, either controlling factor for the Lüders band or for the PLC band, will take the dominant role, thus leading to the distinct competition/coordination between the Lüders band and the PLC band.

Besides the deformation temperature, some previous studies[31,32] revealed that the strain rate and the deformation mode would also affect the macroscopic behaviors (*e.g.*, the band shape and the band propagation behaviors) and the microscopic behaviors (*e.g.*, martensitic transformation kinetics) in medium Mn steels. Although our microscopic mechanistic framework is proposed to explain the effect brought by the different deformation temperatures, we believe that it could also be applied to interpret these behaviors at different strain rates, because the effect brought by higher strain rates is similar to that brought by lower deformation temperatures and vice versa. However, when interpreting the effect brought by the different deformation modes, we think that the current framework should be extended to consider the macroscopic mechanical characteristics of band propagation under each deformation mode. Further research is needed to clarify these effects, since they are important for medium Mn steel's practical application.

ACKNOWLEDGMENTS

This work is supported by the Science Challenge Project, No. TZ2018001, National Science Foundation of China, No. 51671132 and National Key Research and Development Program of China through project No. 2017YFB0304400.

APPENDIX A: EVALUATING THE EFFECT OF THE DEFORMATION TEMPERATURE ON THE DIC MEASUREMENT

The procedure conducted in this study is similar to that proposed in Min *et al.*'s paper.[33] Firstly, the tensile specimen was held for 20 minutes to reach the target temperature and maintain a homogeneous temperature distribution. Secondly, 10 images of each specimen were captured by the DIC cameras. In theory, the equivalent strain of the specimen should be zero, since no load was applied to the specimen during this time. However, the accuracy of DIC strain measurement might be affected by the deformation temperature. Therefore, to evaluate its accuracy, the errors in equivalent strain in those

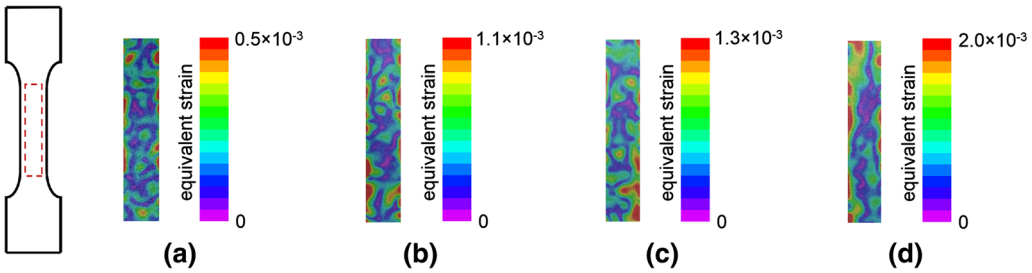

Fig. A1—The DIC-measured equivalent strain distribution in the region denoted by the red dashed box, indicating the errors in equivalent strain at the deformation temperatures of (*a*) 25 °C, (*b*) 55 °C, (*c*) 100 °C and (*d*) 250 °C (Color figure online).

Table A1. The Maximum Errors in Equivalent Stain at Each Deformation Temperature

	25 °C	55 °C	100 °C	250 °C
Maximum error in Equivalent Strain	0.5×10^{-3}	1.1×10^{-3}	1.3×10^{-3}	2.0×10^{-3}

images captured at each deformation temperature (25 °C, 55 °C, 100 °C, and 250 °C) are illustrated separately in Figure A1 and the maximum errors are summarized in Table A1. The results indicate that the deformation temperature only has little effect (less than 2.0×10^{-3}/s) on the DIC measurements.

REFERENCES

1. Y.K. Lee and J. Han: *Mater. Sci. Technol.*, 2015, vol. 31, pp. 843–56.
2. D.W. Suh and S.J. Kim: *Scripta Mater.*, 2017, vol. 126, pp. 63–67.
3. F. Yang, J. Zhou, Y. Han, P. Liu, H.W. Luo, and H. Dong: *Mater. Lett.*, 2020, vol. 258, art. no. 126804.
4. J. Ma, Q. Lu, L. Sun, and Y. Shen: *Metall. Mater. Trans. A*, 2018, vol. 49A, pp. 4404–08.
5. S. Lee and B.C. De Cooman: *Metall. Mater. Trans. A*, 2013, vol. 44A, pp. 5018–24.
6. F. Yang, H.W. Luo, E.X. Pu, S.L. Zhang, and H. Dong: *Int. J. Plast.*, 2018, vol. 103, pp. 188–202.
7. X.G. Wang and M.X. Huang: *J. Iron Steel Res. Int.*, 2017, vol. 24, pp. 1073–77.
8. M.H. Zhang, L.F. Li, J. Ding, Q.B. Wu, Y.D. Wang, J. Almer, F.M. Guo, and Y. Ren: *Acta Mater.*, 2017, vol. 141, pp. 294–303.
9. M.H. Zhang, Q. Tan, J. Ding, H.Y. Chen, F.M. Guo, Y. Ren, and Y.D. Wang: *Mater. Sci. Eng. A*, 2018, vol. 729, pp. 444–51.
10. L Luo, W Li, L Wang, S Zhou, and X Jin: *Mater. Sci. Eng. A*, 2017, vol. 682, pp. 698–703.
11. A. Yilmaz: *Sci. Technol. Adv. Mater.*, 2011, vol. 12, art. no. 063001.
12. B.C. De Cooman, P.J. Gibbs, S. Lee, and D.K. Matlock: *Metall. Mater. Trans. A*, 2013, vol. 44A, pp. 2563–72.
13. J. Han, S.J. Lee, J.G. Jung, and Y.K. Lee: *Acta Mater.*, 2014, vol. 78, pp. 369–77.
14. J.W. Ma, H.T. Liu, Q. Lu, Y. Zhong, L. Wang, and Y. Shen: *Scripta Mater.*, 2019, vol. 169, pp. 1–5.
15. Y Zhang and H Ding: *Mater. Sci. Eng. A*, 2018, vol. 733, pp. 220–23.
16. J.H. Ryu, J.I. Kim, H.S. Kim, C.-S. Oh, H.K.D.H. Bhadeshia, and D.-W. Suh: *Scripta Mater.*, 2013, vol. 68, pp. 933–36.
17. B.H. Sun, N. Vanderesse, F. Fazeli, C. Scott, J.Q. Chen, P. Bocher, M. Jahazi, and S. Yue: *Scripta Mater.*, 2017, vol. 133, pp. 9–13.
18. F. Abu-Farha, X.H. Hu, X. Sun, Y. Ren, L.G. Hector, G. Thomas, and T.W. Brown: *Metall. Mater. Trans. A*, 2018, vol. 49A, pp. 2583–96.
19. X.G. Wang, L. Wang, and M.X. Huang: *Acta Mater.*, 2017, vol. 124, pp. 17–29.
20. X.M. Zhao, Y.F. Shen, L.N. Qiu, X. Sun, and L. Zuo: *Materials*, 2014, vol. 7, pp. 7891–906.
21. H.F. Jiang, Q.C. Zhang, X.D. Chen, Z.J. Chen, Z.Y. Jiang, X.P. Wu, and J.H. Fan: *Acta Mater.*, 2007, vol. 55, pp. 2219–28.
22. R. Sarmah and G. Ananthakrishna: *Acta Mater.*, 2015, vol. 91, pp. 192–201.
23. G.T. Hahn: *Acta Metall.*, 1962, vol. 10, pp. 727–38.
24. M Calcagnotto, D Ponge, E Demir, and D Raabe: *Mater. Sci. Eng. A*, 2010, vol. 527, pp. 2738–46.
25. A. Ramazani, K. Mukherjee, A. Schwedt, P. Goravanchi, U. Prahl, and W. Bleck: *Int. J. Plast.*, 2013, vol. 43, pp. 128–52.
26. A.H. Cottrell: *Lond. Edinburgh Dublin Philos. Mag. J. Sci.*, 1953, vol. 44, pp. 829–32.
27. P.G. McCormigk: *Acta Metall.*, 1972, vol. 20, pp. 351–54.
28. A. van den Beukel: *Phys. Status Solidi A*, 1975, vol. 30, pp. 197–206.
29. R.A. Mulford and U.F. Kocks: *Acta Metall.*, 1979, vol. 27, pp. 1125–34.
30. P.D. Zavattieri, V. Savic, L.G. Hector, Jr, J.R. Fekete, W. Tong, and Y. Xuan: *Int. J. Plast.*, 2009, vol. 25, pp. 2298–330.
31. R. Alturk, L.G. Hector, C. Matthew Enloe, F. Abu-Farha, and T.W. Brown: *JOM*, 2018, vol. 70, pp. 894–905.
32. W. Wu, Y.-W. Wang, P. Makrygiannis, F. Zhu, G.A. Thomas, L.G. Hector, X. Hu, X. Sun, and Y. Ren: *Mater. Sci. Eng. : A*, 2018, vol. 711, pp. 611–23.
33. J. Min, L.G. Hector, Jr., L. Zhang, L. Sun, J.E. Carsley, and J. Lin: *Mater. Des.*, 2016, vol. 95, pp. 370–86.